Seismic evidence for shallow gas-escape features associated with a retreating gas hydrate zone offshore west Svalbard

Sudipta Sarkar,[1] Christian Berndt,[2] Timothy A. Minshull,[1] Graham K. Westbrook,[1,3] Dirk Klaeschen,[2] Douglas G. Masson,[1] Anne Chabert,[1] and Kate E. Thatcher[3]

Received 30 December 2011; revised 20 July 2012; accepted 31 July 2012; published 19 September 2012.

[1] Active gas venting occurs on the uppermost continental slope off west Svalbard, close to and upslope from the present-day intersection of the base of methane hydrate stability (BMHS) with the seabed in about 400 m water depth in the inter-fan region between the Kongsfjorden and Isfjorden cross-shelf troughs. From an integrated analysis of high-resolution, two-dimensional, pre-stack migrated seismic reflection profiles and multibeam bathymetric data, we map out a bottom simulating reflector (BSR) in the inter-fan region and analyze the subsurface gas migration and accumulation. Gas seeps mostly occur in the zone from which the BMHS at the seabed has retreated over the recent past (1975–2008) as a consequence of a bottom water temperature rise of 1°C. The overall margin-parallel alignment of the gas seeps is not related to fault-controlled gas migration, as seismic evidence of faults is absent. There is no evidence for a BSR close to the gas flare region in the upper slope but numerous gas pockets exist directly below the predicted BMHS. While the contour following trend of the gas seeps could be a consequence of retreat of the landward limit of the BMHS and gas hydrate dissociation, the scattered distribution of seeps within the probable hydrate dissociation corridor and the occurrence of a cluster of seeps outside the predicted BMHS limit and near the shelf break indicate the role of lithological heterogeneity in focusing gas migration.

Citation: Sarkar, S., C. Berndt, T. A. Minshull, G. K. Westbrook, D. Klaeschen, D. G. Masson, A. Chabert, and K. E. Thatcher (2012), Seismic evidence for shallow gas-escape features associated with a retreating gas hydrate zone offshore west Svalbard, *J. Geophys. Res.*, *117*, B09102, doi:10.1029/2011JB009126.

1. Introduction

[2] Methane hydrates are stable in Arctic continental margin sediments in water depths greater than 300–400 m [*Kvenvolden et al.*, 1993; *Kvenvolden*, 1993; *Hester and Brewer*, 2009]. The stability of methane hydrates is sensitive to changes in pressure and temperature such that a drop in pressure or increase in temperature may lead to dissociation of hydrates and release of gas. Methane that reaches to the atmosphere may contribute to climate change because methane is a potent greenhouse gas [*Houghton et al.*, 2001; *Isaksen et al.*, 2011]. In the present-day, ocean warming is manifested in the Arctic by rapid loss of Arctic sea ice [*Comiso et al.*, 2008; *Piechura and Walczowski*, 2009]. Hydrates in the Arctic continental slope remain particularly sensitive to climate change because future climate change (such as increased temperature) is likely to be felt more acutely than at the lower latitudes [*Houghton et al.*, 2001]. Based on future climate projections, modeling results already indicate that shallow Arctic regions influenced by North Atlantic water inflow may undergo hydrate destabilization in the next 100 years [*Biastoch et al.*, 2011]. Despite the concern about warming induced hydrate dissociation in the Arctic, there is little present-day field-based evidence.

[3] Methane hydrate occurrences are well known in the western continental margin of Svalbard [*Posewang and Mienert*, 1999; *Vanneste et al.*, 2005; *Westbrook et al.*, 2008; *Chabert et al.*, 2011; *Fisher et al.*, 2011]. During cruise JR211 in August–September 2008, a sonar survey revealed numerous plumes of gas bubbles emanating from the seafloor on the upper continental slope (Figures 1b and 2), with water in the plumes showing elevated concentration of methane [*Westbrook et al.*, 2009]. The high concentration of gas seeps was discovered in a narrow depth range on the upper slope, which lies near and immediately upslope of the predicted landward limit of the methane hydrate stability zone (MHSZ) located at ~400 m water depth [*Westbrook et al.*, 2009]. A warming trend in the West Spitsbergen Current, a northward flowing branch of the North Atlantic current off west Svalbard, has been observed over the past three decades (1975–

[1]National Oceanography Centre, Southampton, University of Southampton, Southampton, UK.
[2]GEOMAR Helmholtz-Zentrum für Ozeanforschung, Kiel, Germany.
[3]School of Geography, Earth and Environmental Sciences, University of Birmingham, UK.

Corresponding author: S. Sarkar, National Oceanography Centre, Southampton, University of Southampton, European Way, SO14 3ZH Southampton, UK. (ss1g08@noc.soton.ac.uk)

©2012. American Geophysical Union. All Rights Reserved.
0148-0227/12/2011JB009126

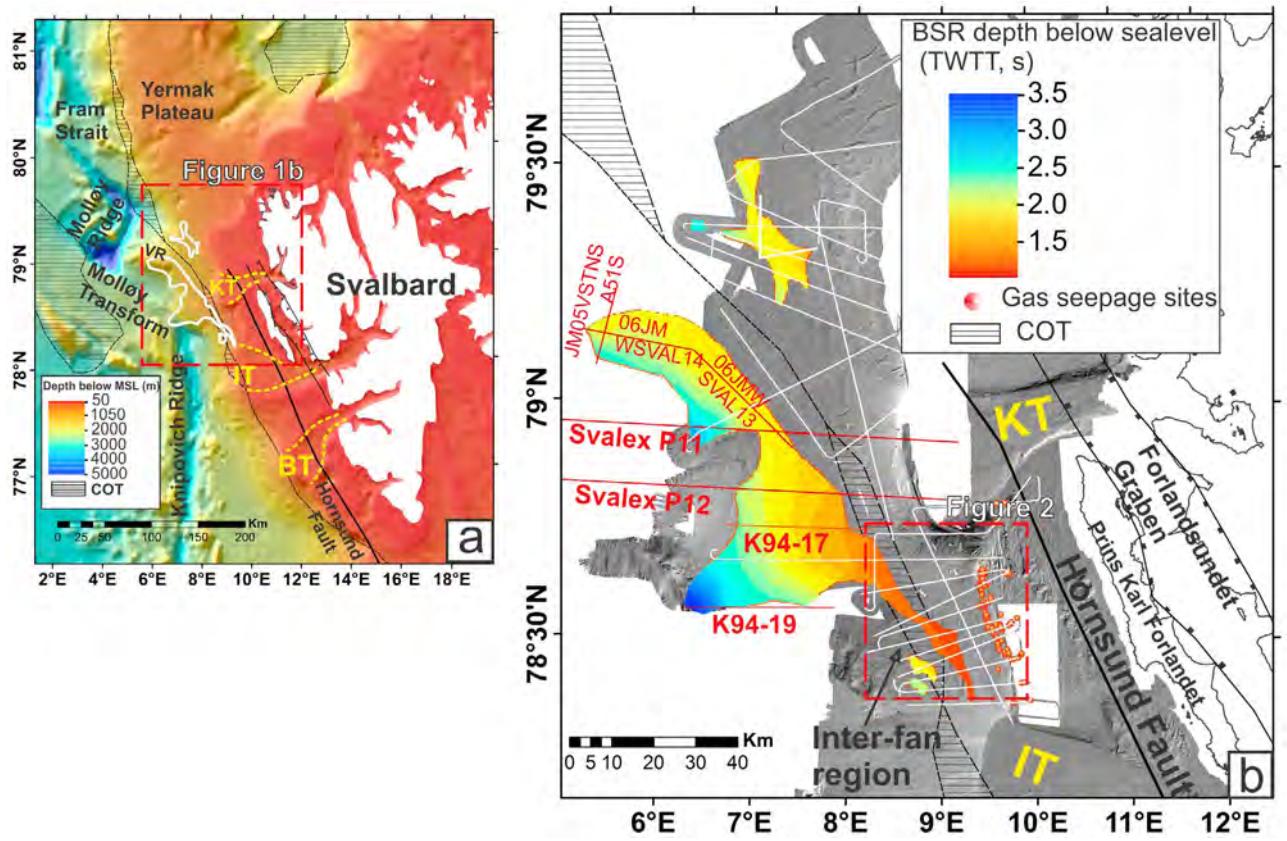

Figure 1. West Svalbard continental margin and the study area with part of the International Bathymetric Chart of the Arctic Ocean [*Jakobsson et al.*, 2008]. (a) Knipovich Ridge-Molløy Transform Fault-Molløy Ridge constitutes the mid-oceanic ridge and transform fault system in the west. Vestnesa Ridge (VR) is a contouritic drift system. Kongsfjorden cross-shelf trough (KT), Isfjorden cross-shelf trough (IT) and Bellsund cross-shelf trough (BT) dissect the shelf. The solid white line represents the gas hydrate province inferred from a seismic bottom simulating reflector (BSR). The Continent-Ocean Transition (COT) is from *Engen et al.* [2008]. (b) The BSR extent and depth map (s, Two Way Travel Time) displayed on shaded relief bathymetric image. The interpretation of the BSR is based on JR211 seismic lines (white solid) and previous studies (red lines). K94-17 and K94-19 are from *Posewang and Mienert* [1999], JM lines are from *Frantzen* [2008], Svalex lines are from *Hustoft et al.* [2009]. Gas seeps determined from EK60 sonar survey during JR211 are located on the upper continental slope and shelf.

2008) based on summer Conductivity-Temperature-Depth (CTD) data [e.g., *Holliday et al.*, 2008]. Analyses of CTD data collected in the summers of 2000–2006 [*Walczowski and Piechura*, 2007], year-round mooring data [*Schauer et al.*, 2008] and planktic foraminiferal assemblages of a sediment core from Fram Strait [*Spielhagen et al.*, 2011] indicate that Atlantic Water temperature at the beginning of the 21st century is higher than for the past 2000 years. Based on hindcast simulations, *Biastoch et al.* [2011] inferred a weak long-term warming trend (<0.005°C yr^{-1}) of Atlantic Water at water depths of 416–793 m over the past few decades. However, *Westbrook et al.* [2009] showed a more pronounced warming of the intermediate water at shallower water depths (300–450 m) during the past 30 years. For the period 1975–2008, temperature measurements from the deepest 10 m of CTD casts in the gas flare region show an overall 1°C warming of the bottom water [*Westbrook et al.*, 2009]. The increase of seabed temperature from 2°C to 3°C will have deepened the upper limit of methane hydrate stability at the seabed by about 30 m to 400 m water depth at present and caused its intersection with the seabed to recede about 1200 m down the continental slope, which dips westward at about 1.25° in the vicinity of the gas seeps and destabilize hydrate that was previously within the MHSZ [*Westbrook et al.*, 2009; *Thatcher and Westbrook*, 2011].

[4] Marine gas seeps can be controlled by several geological processes. It has not yet been confirmed whether the seafloor seeps on the upper continental slope in west Svalbard are sourced from hydrate dissociation or whether other mechanisms control gas expulsion along a narrow corridor, such as faults terminating close to the seafloor. Here, we determine the subsurface gas distribution and gas migration pathways in order to establish the link between the spatial distribution of seeps and sub-seabed gas accumulations. Using seismic and multibeam bathymetric data, we examine potential mechanisms that control fluid focusing, such as structurally and stratigraphically controlled gas migration, degassing due to gas hydrate dissociation and the seabed vent structures (such as pockmarks, ploughmarks) over the high-density gas seepage region offshore west Svalbard. The

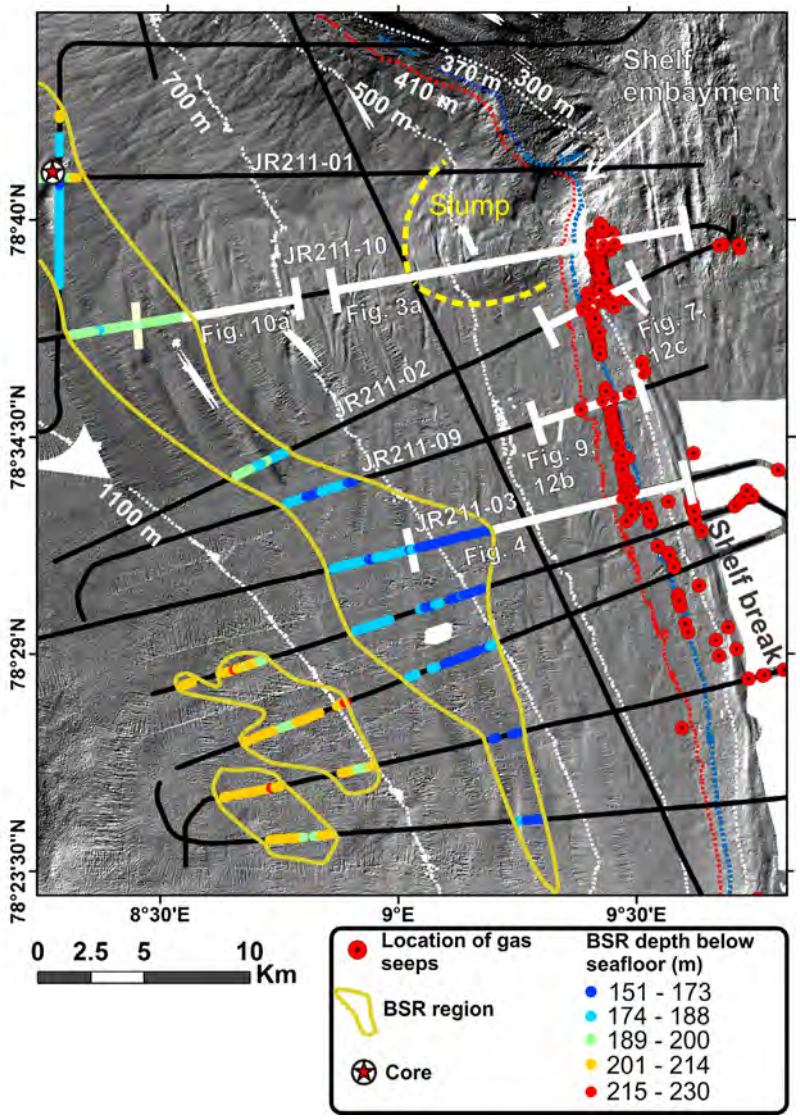

Figure 2. Shaded relief image of JR211 multibeam data with seafloor gas seepage locations and JR211 seismic lines (black) in the inter-fan region between KT and IT. White lines mark the locations of the seismic reflection profiles shown in this paper. Gas hydrate was recovered from a sediment core at the site shown in the figure. The 370 and 410 m bathymetric contours represent the upper limit of modeled base of methane hydrate stability (BMHS) at 2°C and 3°C bottom water temperatures respectively.

objectives of this study are – (1) to assess the extent to which degassing is caused by hydrate dissociation, and (2) to delineate fluid migration pathways within the shallow marine sediments in the upper continental slope off west Svalbard and explain the shallow focusing of gas escape over a narrow range of water depths.

2. The West Svalbard Margin

[5] The Pliocene–Pleistocene development of the continental margin was primarily shaped by advances and retreats of the Svalbard-Barents Sea ice sheet [*Solheim et al.*, 1996; *Knies et al.*, 2009]. The present-day Svalbard shelf break represents the approximate maximum extent of ice sheet expansion. Within the ice sheet, fast-flowing ice streams were confined to the cross-shelf troughs, such as Kongsfjorden and Isfjorden cross-shelf troughs (Figures 1a and 1b). The ice streams deposited prograding glacial wedges called Trough Mouth Fans (TMFs) in front of the troughs. The Kongsfjorden Trough Mouth Fan (KTMF) and Isfjorden Trough Mouth Fan (ITMF) were deposited in front of the corresponding cross-shelf troughs [*Dowdeswell and Elverhøi*, 2002; *Sarkar et al.*, 2011]. The fans are represented by prograding glacial debris flows [*Vorren and Laberg*, 1997; *Vorren et al.*, 1998; *Sarkar et al.*, 2011]. While glacigenic sedimentation was predominant in the shelf and upper continental slope, the distal slope was influenced by bottom water currents, leading to the development of contourite drifts [*Eiken and Hinz*, 1993]. Our study area (Figure 1b, inset and Figure 2) is located in the inter-fan region east of the Knipovich Ridge, between the Kongsfjorden and Isfjorden cross-shelf troughs, and seaward of the shelf break (Figures 1a and 1b).

[6] A bottom simulating reflector (BSR), which marks the base of the gas hydrate stability zone (GHSZ) [*Shipley et al.*, 1979; *Stoll and Bryan*, 1979] occurs in the continental slope offshore west Svalbard [*Vogt et al.*, 1994; *Posewang and Mienert*, 1999; *Westbrook et al.*, 2008; *Hustoft et al.*, 2009; *Chabert et al.*, 2011]. The BSR area is bounded to the west by the WNW-ESE trending Molløy Transform Fault and extends over the Vestnesa ridge (VR in Figure 1a, water depth ~1200–1300 m), which represents a sediment drift system [*Eiken and Hinz*, 1993; *Howe et al.*, 2008]. The eastern boundary of BSR occurrence appears to be limited by the influence of glacial sediments, probably due to their low permeability [*Vanneste et al.*, 2005]. Seeps are also well-known from numerous pockmarks that occur at the crest of the Vestnesa ridge [*Vogt et al.*, 1994; *Hustoft et al.*, 2009]. Here, the presence of a fluid migration system is indicated by seismic chimneys terminating in these pockmarks [*Vogt et al.*, 1994; *Petersen et al.*, 2010].

3. Data and Methods

3.1. 2D Multichannel Seismic (MCS) Data and Processing

[7] MCS lines (Figure 2) were acquired using a 96 channel streamer (group spacing 6.25 m) with an active length of 600 m and maximum offset of 650 m. The seismic source consisted of two generator-injector (GI) air guns each with a volume of 150 cubic inch (45 cubic inch generator and 105 cubic inch injector) at a depth of 3 m. The shot interval was 4 s, resulting in a mean shot distance of 12.5 m. Preprocessing steps included sorting the data into the common midpoint (CMP) domain with CMP bin spacing of 3.125 m, deleting noisy traces, noise attenuation (data adaptive methods to suppress incoherent noise), data interpolation, and F-K demultiple to attenuate water-bottom multiple. We carried out pre-stack depth migration in order to obtain a reliable long wavelength background velocity model. The depth imaging sequence consisted of several iterations (typically five) of Kirchhoff pre-stack depth migration and depth-focusing analysis (DFA). DFA was performed on every one-hundredth common reflection point gather, so the lateral resolution of the velocity model is ~300 m. The derived velocity field was smoothened over a 25 m horizontal and 40 m vertical grid. The final velocity grid obtained from iterative depth migration was converted into root mean square (RMS) and interval velocities in the time domain. We also carried out pre-stack Kirchhoff time migration with the pre-processed common offset gathers using RMS velocities in the time domain that were derived from pre-stack depth migration velocity analysis. The final version of the RMS velocity was refined with residual moveout (RMO) correction on every CMP and converted to interval velocity for interpretation. The relative error or the sensitivity of RMO analysis is dependent on the streamer length, reflector depth, background velocity and bandwidth of the data. For example, in the uppermost slope (water depths 350–400 m), RMO within a range of $\pm$6 ms (when the wavelet length is 12 ms) at the maximum offset may still remain unresolved. The associated velocity uncertainties are estimated at 3–5% at 0.60–1.00 s TWTT and 8–10% at 1.00–1.50 s TWTT (based on solving the hyperbolic moveout equation).

3.2. Multibeam Bathymetric Data

[8] Multibeam bathymetric data were recorded by Kongsberg Simrad EM120 system (191 beams and 12 kHz frequency) during the JR211 cruise, covering the slope over a depth range of 50–3200 m. This data was gridded with a horizontal cell size of 20 m. Additional multibeam bathymetric data covering the shelf (water depths between 50 m and 350 m) were acquired by the Norwegian Hydrographic Service [*Ottesen et al.*, 2007] and these data were gridded with a 2 m horizontal cell size. We produced shaded relief images (illumination from NW) from both these bathymetric data sets.

[9] We used seafloor gas seepage locations (Figures 1b and 2) obtained from the Simrad EK60 echogram images that captured the gas seeps using the ship's split-beam sonar system operating at 38 kHz, which was capable of providing three-dimensional locations of the bubbles and allowed us to map the origin of the gas plumes emanating from the seafloor. Part of the EK60 sonar image showing the high amplitude backscatter from the rising bubbles is shown in Figure 1 by *Westbrook et al.* [2009]. In this paper we show the gas plumes on the seismic profiles which are within 10 m distance of the seismic profiles.

4. Results

4.1. Stratigraphy

[10] The glacimarine Pliocene-Pleistocene succession of the inter-fan region is represented by three seismic stratigraphic Units - I (youngest), II and III (oldest). Reflector A4 (age between 1.5 and 0.99 Ma) separates Units I and II, whereas A5 separates Units II and III. A6 (age ~2.8–2.6 Ma) represents the base of Unit III. Unit IV is the sequence below A6 and above the first seafloor multiple. This stratigraphic nomenclature is adopted from *Sarkar et al.* [2011].

[11] Three types of seismic facies are commonly observed in the seismic sections – (a) prograding foresets, (b) transitional inter-fan facies and (c) well-stratified facies. Westward dipping prograding foresets occur under the shelf within Unit I (profile JR211–10, Figures 3a and 3b). The progradational system is a consequence of slow ice sheet expansion and low supply of glacial debris. The prograding foresets grade into a transitional inter-fan facies below the uppermost slope, between 300 and 400 m water depth (profile JR211–03, Figure 4a). The transitional facies displays incoherent reflections interlayered with stratified and contorted reflections (profile JR211–03, Figure 4b). We presume that the incoherent reflections represent glacigenic deposits (e.g., glacial diamicton) and stratified reflections result from hemipelagic materials and deposits from glacial suspension plumes. In the upper slope (water depths 450–600 m), channels (150–500 m wide and 25–30 m deep) are commonly observed within Unit I, with some cutting through its base into Unit II (Figure 4b). Well-stratified facies and climbing waves occur in the distal slope (within Units I–IV in profile JR211–03, Figure 4a) and represent marine contouritic deposits.

[12] A mass transport complex (slump) showing incoherent reflections (Figure 3a) occurs within Unit I below the upper slope of the northern inter-fan region (internal

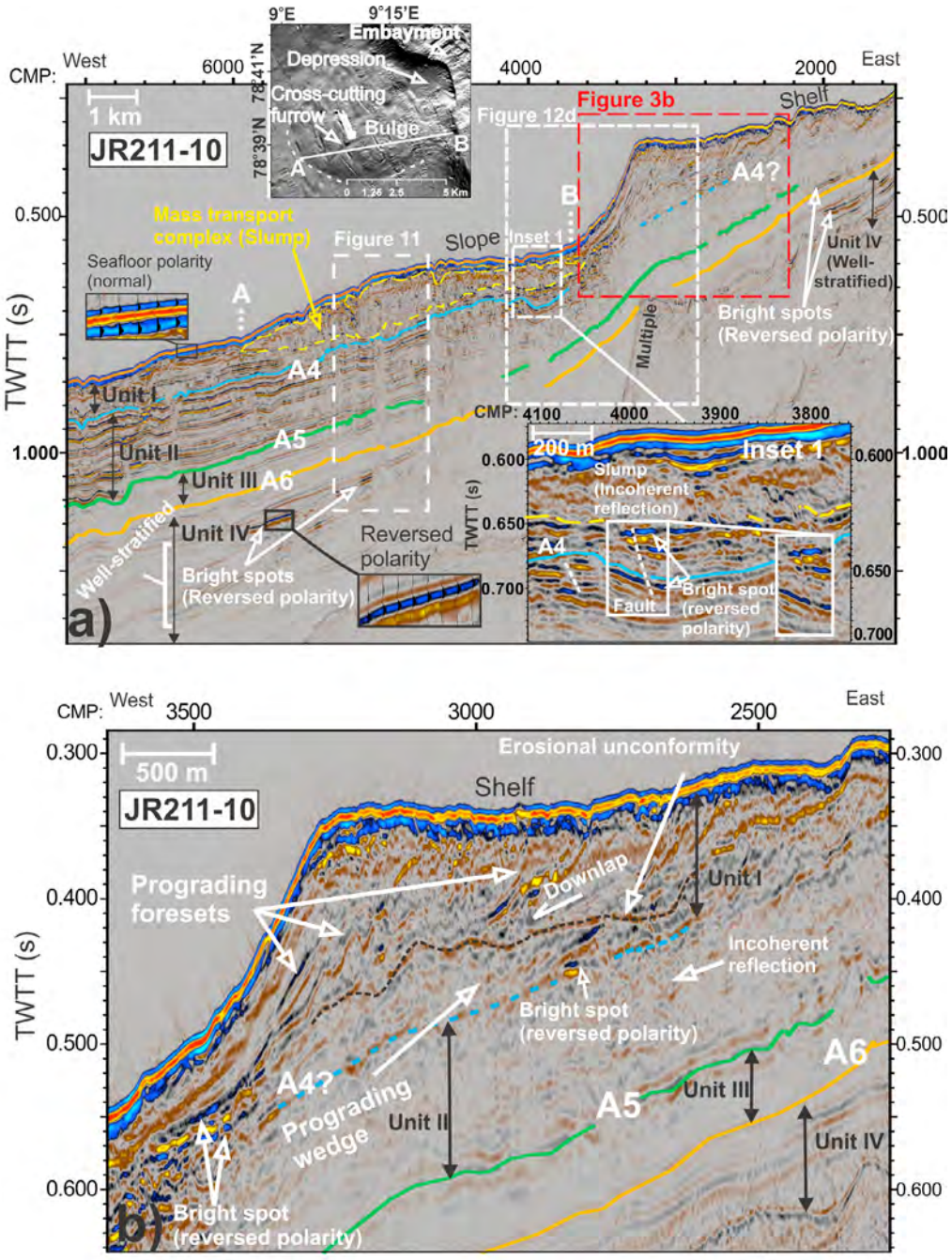

Figure 3. Seismic line JR211-10 illustrating the key seismic reflectors (A4–A6) and the various seismic facies. (a) Shaded relief bathymetric image (location Figure 2) in an inset shows a topographic bulge and profile AB shows a slump with internally contorted and incoherent reflections within Unit I. Units III and IV are represented by well-stratified facies. Bright spots with reversed polarity (with respect to the seafloor polarity) are seen within Unit IV beneath the slope as well as shelf. Inset 1 shows a minor reverse fault below the slump and bright spots with reversed polarity are juxtaposed against the fault. (b) Seismic facies variation in the shelf region (location marked by a red box in Figure 3a). Unit II is characterized by zones of incoherent reflections. Unit I shows prograding foresets. An erosional unconformity separates an underlying prograding wedge from the overlying prograding and downlapping foresets. Bright spot with reversed polarity exists at the base of prograding wedge.

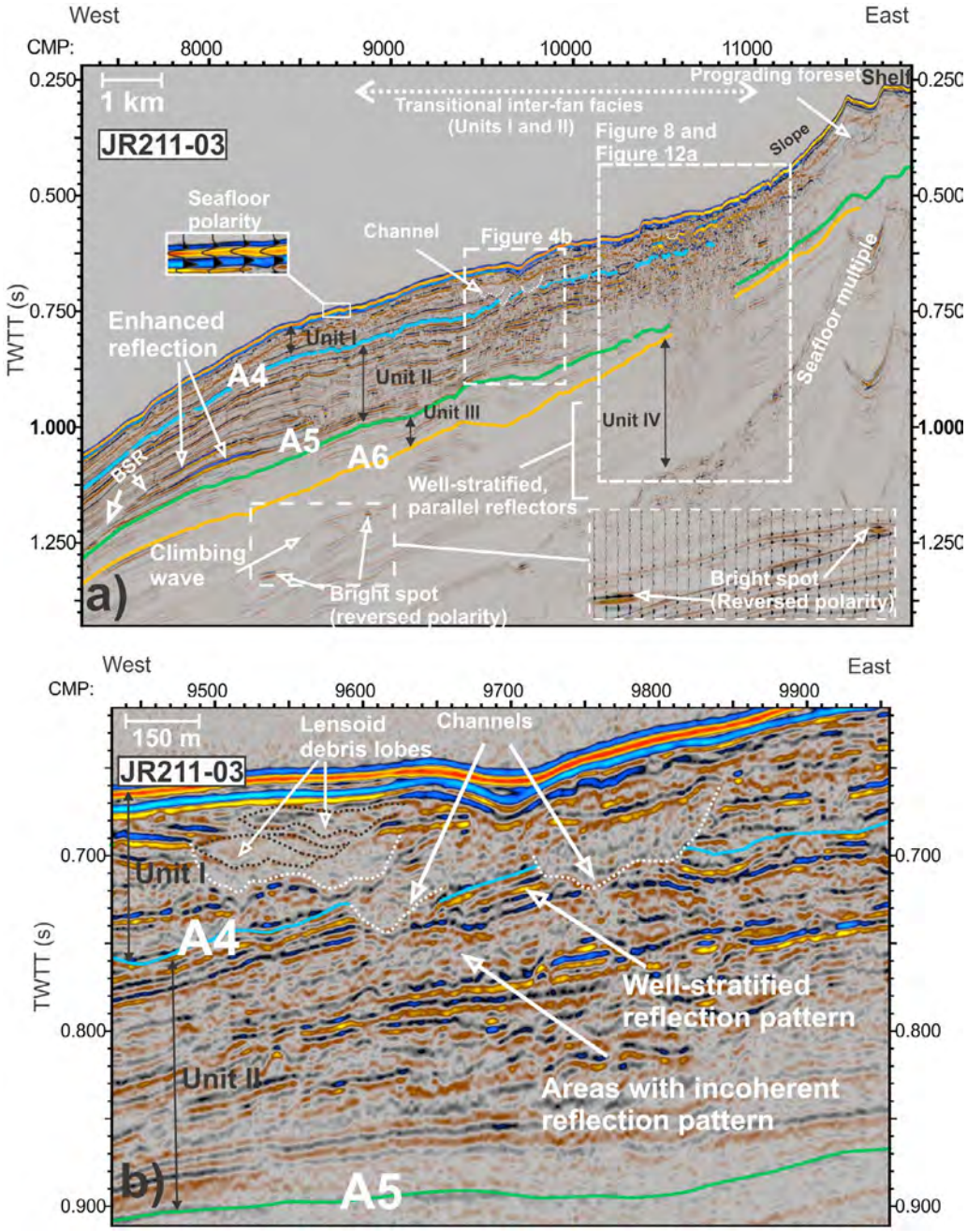

Figure 4. Seismic line JR211-03 illustrating stratigraphic details of the inter-fan region. (a) Well-stratified and climbing wave facies are seen in Unit IV. Bright spots with reversed polarity are seen at the crests of these climbing waves (see inset). Unit I shows prograding foresets beneath the shelf that laterally grade into transitional inter-fan facies beneath the slope. A BSR is seen in the mid slope where it crosscuts the well-stratified, dipping reflectors of Unit II, but it cannot be traced to the uppermost slope. Reflection brightening occurs below the BSR. (b) Transitional inter-fan facies within Units I and II is characterized by incoherent reflection zones (location in Figure 4a). Erosional channels are present within Unit I, with some cutting into the underlying Unit II. The channels are filled by chaotic reflection packages or stacked lobate-shaped bodies interpreted as debris lobes.

structures in Figures S1 and S2 in the auxiliary material).[1] Reflectors of Unit II below the slump show evidence for minor reverse faults (Figure 3a, Inset 1).

4.2. Seafloor Morphology

[13] Geomorphological features on the seafloor may locally influence the locations of the gas seeps and they need to be studied in order to understand any spatial correlation

[1]Auxiliary materials are available in the HTML. doi:10.1029/2011JB009126.

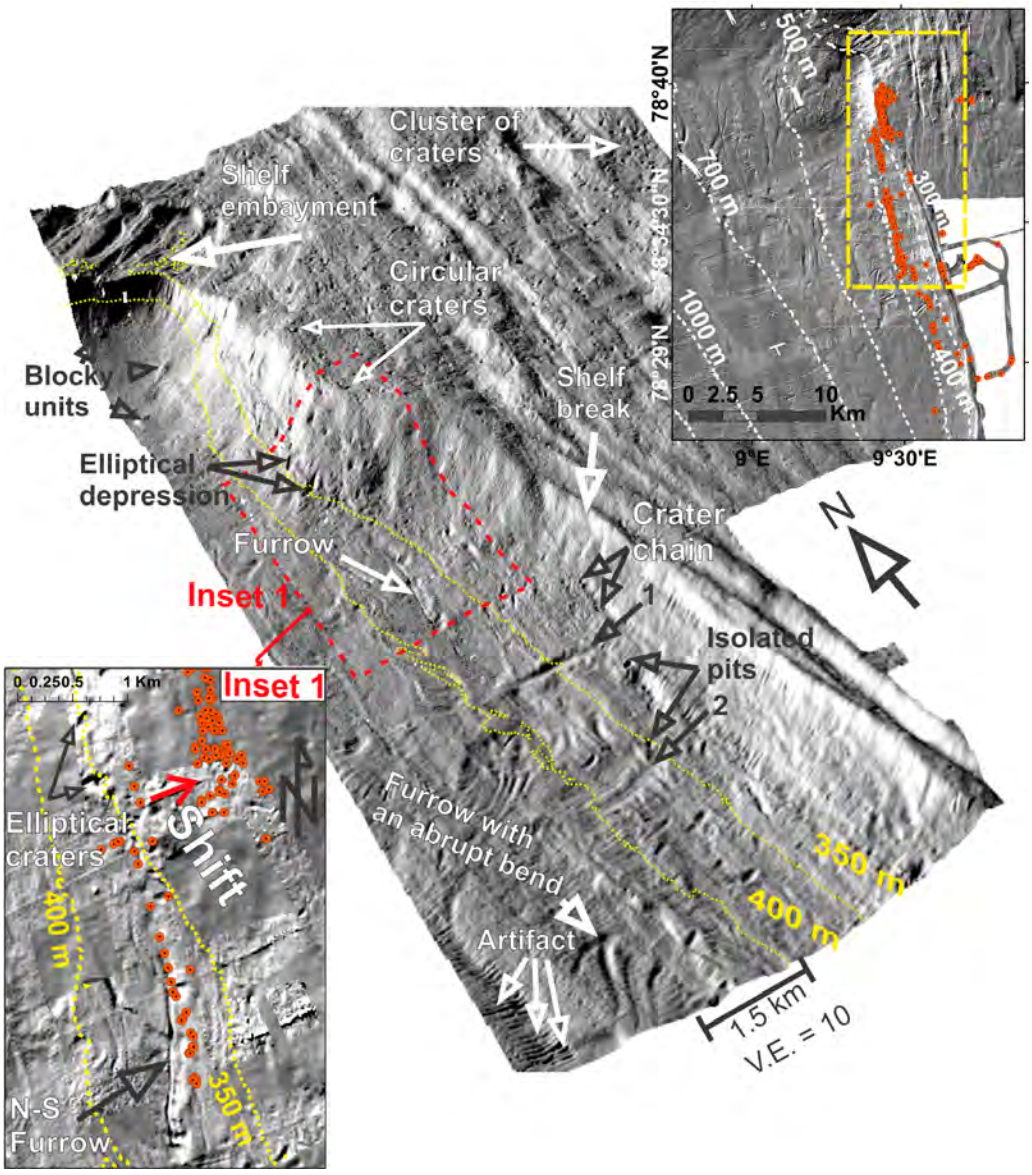

Figure 5. A three-dimensional rendition of the shaded relief bathymetric image (located within a yellow dotted box shown in a map at the upper right hand corner) showing blocky bodies west of the shelf embayment, elliptical depressions or craters on the upper slope, pits, a crater chain and furrows. A furrow shows an abrupt bend in the southwest corner of the image. Features marked as 1 and 2 are cross-slope oriented furrows. The shelf break is represented by a ridge. Inset 1 shows gas seeps coincide with a N-S trending ploughmark (located between 370 and 410 m water depths, which correspond to the postulated BMHS limits at 2°C and 3°C bottom water temperatures respectively) and a shift in the location of seeps toward the shelf break.

between the seeps and these features. Therefore, we describe below the morphology of some relevant features.

[14] A convex upward topographic bulge (Figure 3a, shaded relief bathymetric image) is observed slopeward of the shelf embayment and in the northeastern part of the study area. A few blocky units (200 m long, 150 m wide and ~2 m high, Figure 5) exist within the depression that separates the bulge from the shelf break. Based on our seismic data and work of *Vanneste et al.* [2007], we identify the bulge and blocky bodies as a slump and slump blocks respectively. We do not find any evidence for gas seeps above the slump area (Figure 2).

[15] Several linear and curvilinear seafloor furrows incise the seabed seaward of the embayment area (Figure 3a, shaded relief bathymetric image) and in the inter-fan area (Figure 5). They are V-shaped in profile, 15–175 m wide (average width ~45 m), 2–10 m deep and a few 100 m to several km long. They are generally slope-parallel but a few are oriented across-slope (e.g., Features 1 and 2 in Figure 5). Some of them crosscut each other (shaded relief bathymetric image in Figure 3a) and also show abrupt bends (Figure 5). Following *Hohbein and Cartwright* [2006] and *Bellec et al.* [2008], we interpret the furrows as iceberg ploughmarks.

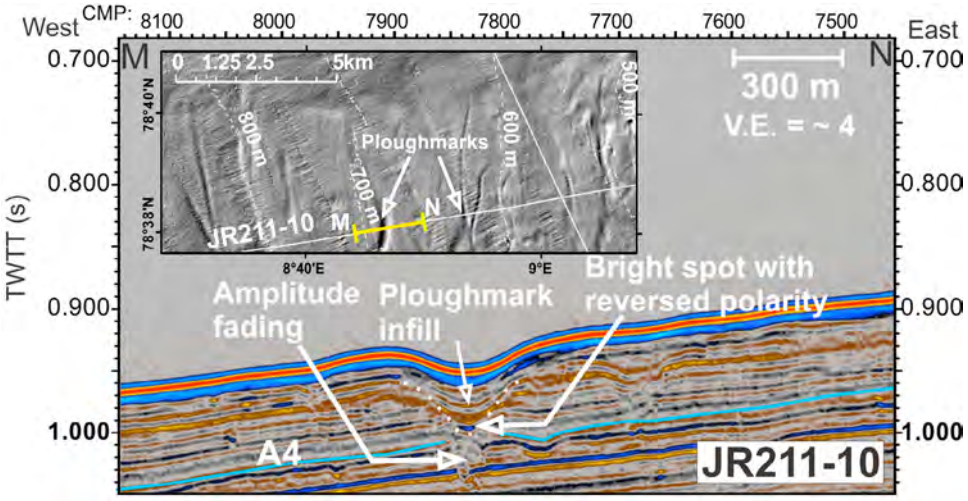

Figure 6. Seismic line JR211-10 (MN in the bathymetric image and its location in Figure 2) showing a V-shaped furrow (ploughmark). An erosional contact is seen at the base (marked by white dots) along with a bright spot with reversed polarity. Amplitude disturbance is seen below the bright spot. The incision is filled with sediments.

They are a result of seabed erosion by drifting iceberg keels. Seismic profile JR211–10 shows that a ploughmark (Figure 6) has been filled with sediments. There are places in the inter-fan region where gas seeps coincide with parts of ploughmarks, such as a subtle N–S ploughmark (Figure 5, Inset 1) in the north.

[16] Several circular (diameter ~125 m) and elliptical (long axis ~270 m) crater-like depressions and small pits (~100 m radius, and ~10 m deep) exist on the shelf and upper slope of the inter-fan region. Circular depressions are clustered in the shelf region (Figure 5) and rarely in a chain-like fashion. Isolated pits are observed close to ploughmarks (Figure 5). Ploughmarks in conjunction with craters and crater chains could be due to indentations made by oscillating and drifting iceberg keels as described by *Bass and Woodworth-Lynas* [1988]. Gas seeps occur above circular craters near the shelf break (Figure 5, Inset 1) but are absent from the large elliptical craters and small pits on the uppermost slope.

4.3. Seismic Observations Associated With the Fluid Flow System

4.3.1. Bright Spots

[17] Bright spots appear in several places in the slope perpendicular sections and occur at various stratigraphic levels. Deeper bright spots with reversed polarity occur within the well-stratified sequence in Units III and IV beneath the upper slope and shelf (Figure 3a), with some located at the crests of climbing waves (Figure 4a). Bright spots with reversed polarity also exist below the upper slope within Units I and II. Within Unit I, bright spot with reversed polarity occurs at the base of the slump deposit in profile JR211–10 (Figure 3a, Inset 1). Numerous shallow bright spots are scattered within Unit I below water depths 0.50–0.56 s TWTT (~310–400 m), such as in profiles JR211–02 (Figure 7), JR211–03 (Figure 8) and JR211–09 (Figure 9). The absolute reflection coefficients for the reversed polarity scattered bright spots (Figure 8) range from 0.08 to 0.5 with a mean of 0.25 and $\sigma = 0.01$ (method for determining absolute reflection coefficient is described in Text S1 in the auxiliary material). The lowest reflection coefficient value can be explained by a low P wave velocity (1300 ms^{-1}) layer underlying a layer of relatively higher velocity 1500 ms^{-1} (assuming density of the layers are similar). The higher values may result from interference and/or focusing effect. We interpret this low velocity to be caused by the presence of free gas. Reflections from the walls and base of a channel within Unit II in profile JR211–09 (below water depth 0.53–0.56 s TWTT (~400 m)) are enhanced by the presence of bright reflections (Figure 9).

[18] Beneath the outer shelf within Unit I, a bright spot with reversed polarity occurs at the base of a prograding wedge (Figures 3b and 7). In profile JR211–02, the westward-dipping prograding reflector F shows reversed polarity and amplitude brightening in several places (Figure 7). Within the prograding 'top wedge', overlying reflector F in Unit I, a shallow foreset shows high amplitudes with predominantly reversed polarity (Figure 7, Inset 1). Near the toe of the prograding wedge, a mound-shaped wave-like feature, interpreted to be sediment drift, fills an erosional scar in JR211–02 (Figure 7, Inset 1). The base and crest of this drift show high amplitudes with reversed polarity.

4.3.2. BSR

[19] We identify a bottom-simulating reflector (BSR) in our seismic data based on its reversed polarity, parallelism to seafloor and crosscutting relationship with the strata (Figure 10a). We interpret reflection brightening below the BSR (Figures 4a and 10a) to be due to the presence of free gas. The BSR cannot generally be detected in water depths shallower than about 700 m beneath the upper continental slope (Figure 4a). While previous studies [*Vanneste et al.*, 2005] located the BSR province west of the KTMF, our new data show that the BSR also continues south into the inter-fan region (Figures 1b and 2). A sediment core (location in Figure 2) collected during the cruise JR211 confirmed physical presence of gas hydrate [*Fisher et al.*, 2011].

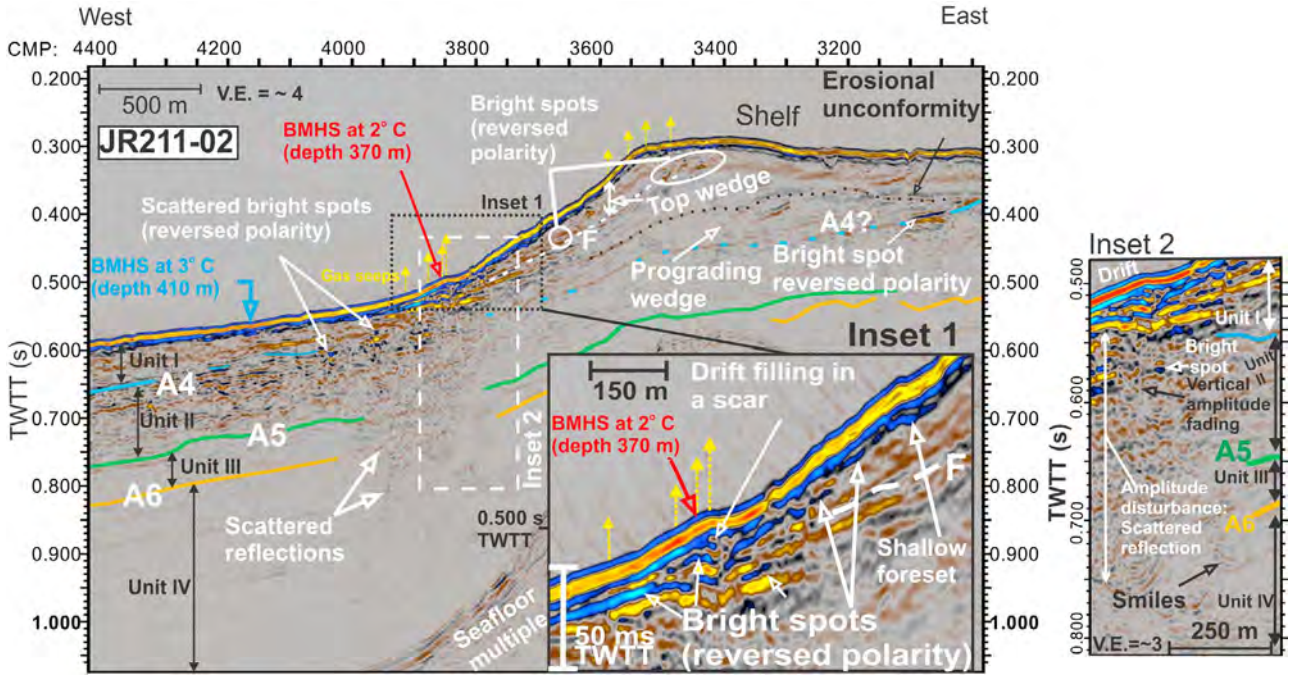

Figure 7. Seismic anomalies in line JR211-02. A bright spot with reversed polarity is present at the base of a prograding wedge within Unit I beneath the shelf. Reflection brightening is seen at several isolated places along reflector F and also along a shallow foreset (Inset 1). A drift mound fills an erosional scar on the upper slope (Inset 1) and bright spots with reversed polarity occur at the crest and base. Scattered bright spots are also present at the base of Unit I below the upper slope. Gas seeps are clustered into two locations, on the drift mound and at the shelf break. An area of scattered reflections occurs within Units I–III beneath the upper slope (Inset 2). This zone shows near-vertical linear amplitude fading and scattered bright spots occur near the top. Isolated smile-like features occur below A6 (Inset 2). The "Smiles" result from imperfectly migrated (relatively high migration velocity) seismic energy scattered from shallow out-of-plane gas pockets.

4.3.3. Seismic Chimneys

[20] We interpret the seismic chimneys as vertical or near-vertical zones with lower reflection strength than the surrounding sedimentary reflectors. In some instances, internal reflections are preserved but with reduced amplitude. For example, near CMP 8250 in Figure 10a, a chimney terminates at reflector A4. The chimney has a width of ~250 m. It shows prominent reflection up-bending and internal amplitude reduction (Figure 10b). Another deep-rooted chimney at water depth ~0.625 s TWTT (~450 m) shows internal faulting and amplitude suppression (Figure 11). It appears to originate at the level of a bright spot within Unit IV.

4.3.4. Scattered Reflections Beneath the Upper Slope of the Inter-Fan Region

[21] Scattered reflections (Profiles JR211–03 (Figure 8) and JR211–02 (Figure 7, Inset 2)) and vertical/near-vertical linear or curvilinear areas of amplitude dimming (Figure 8 (Inset 1) and Figure 7 (Inset 2)) occur within Units I and II beneath the upper slope. Areas with scattered reflection show poor reflection continuity. Scattered reflections may arise from disrupted sedimentary fabric as a result of gas migration, probably through fracture networks. The pattern of scattering is less dense than in what is often called 'acoustic turbidity', which is also interpreted as evidence for the presence of gas [e.g., *Judd and Hovland*, 1992]. Following *Haacke et al.* [2009], the linear areas of amplitude fading could be due to gas migration through fractures. We also observe a few patchy occurrences of scattered reflections within the deeper stratigraphic units (Units III and IV, Figure 8). The depths of these deeper scatterers below the seabed are not as great as they appear on the sections. Based on migration velocity analysis, we interpret them as seismic energy scattered from shallow gas pockets that are out-of-plane of the 2D seismic lines.

4.3.5. Velocity Anomalies Beneath the Upper Slope

[22] Seismic P wave interval velocities (V_P) obtained by DFA during pre-stack depth migration and corrected for residual moveout show shallow low-velocity zones below the upper continental slope. For example, low-velocity anomalies are encountered in seismic lines JR211–03 (Figure 12a) and JR211–09 (Figure 12b) below water depths of 0.50–0.60 s TWTT (375–450 m). In JR211–03 (Figure 12a) the low-velocity area is ~1 km wide, ~0.32 s TWTT (~345 m) deep and extends down to Unit IV. In profile JR211–03 the low-velocity zone (Figure 12a) corresponds to an area of scattered reflections within Units I–II (Figure 8). An area of scattered incoherent reflections in Units III and IV also displays a low-velocity anomaly (Figure 12a). Isolated low-velocity pockets coincide with the scattered bright spots in JR211–02 under the upper slope (Figure 12c). A low-velocity anomaly also exists within a channel system in Unit II (line JR211–10, Figure 12d). The channel is ~450 m wide and ~65 m deep,

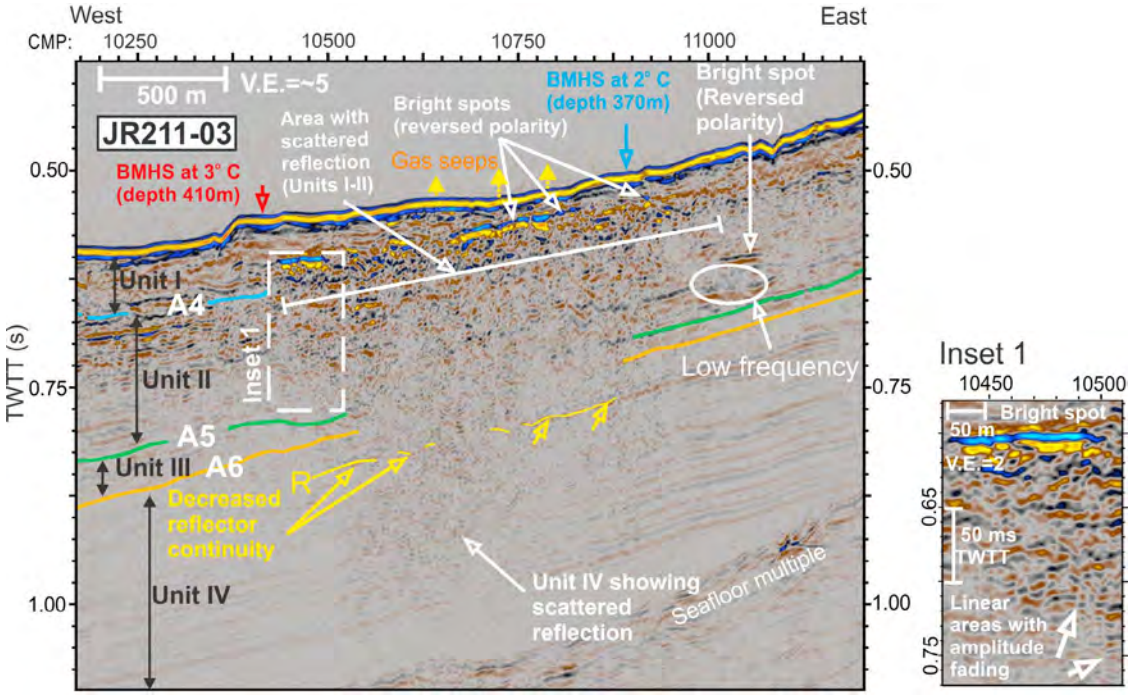

Figure 8. Seismic line JR211-03 (location in Figure 4) illustrating seismic anomalies associated with gas accumulation and migration beneath the upper slope. Several scattered bright spots with reversed polarity are present within Unit I. A broad zone with scattered reflections exists within Units I–II. This zone shows incoherent reflections, near-vertical linear areas with amplitude fading (Inset 1) and bright spots (reversed polarity) with underlying low frequency. In Units III–IV a patchy incoherent reflection zone shows decreased reflector continuity (e.g., reflector R).

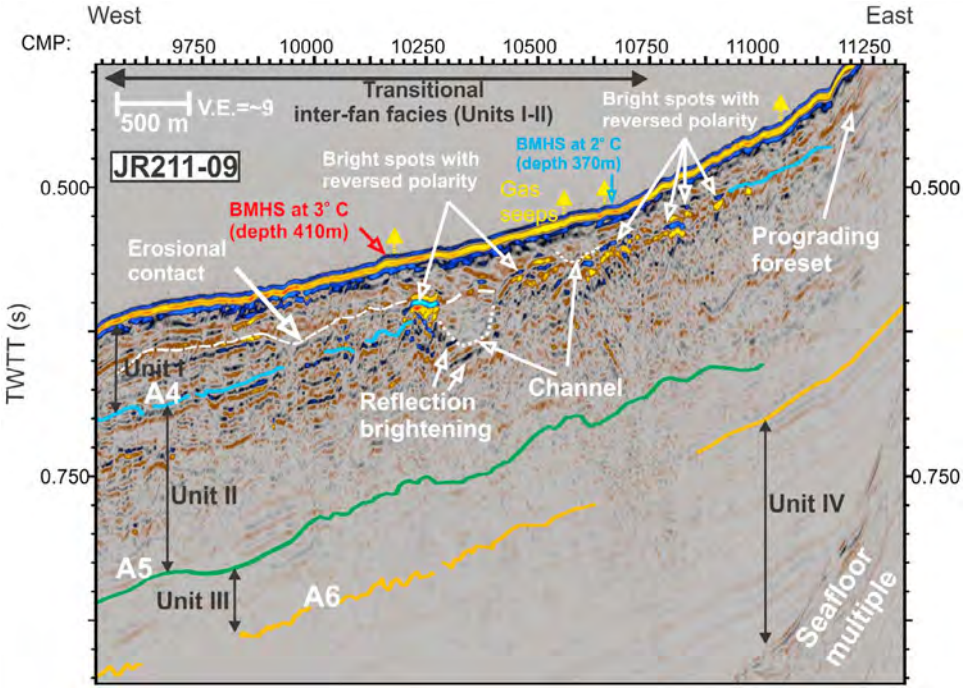

Figure 9. Seismic line JR211-09 showing seismic anomalies beneath the upper continental slope. Numerous shallow bright spots with reversed polarity are present in Unit I. A few erosional channels are present at the base of Unit I with the underlying strata showing reflection brightening.

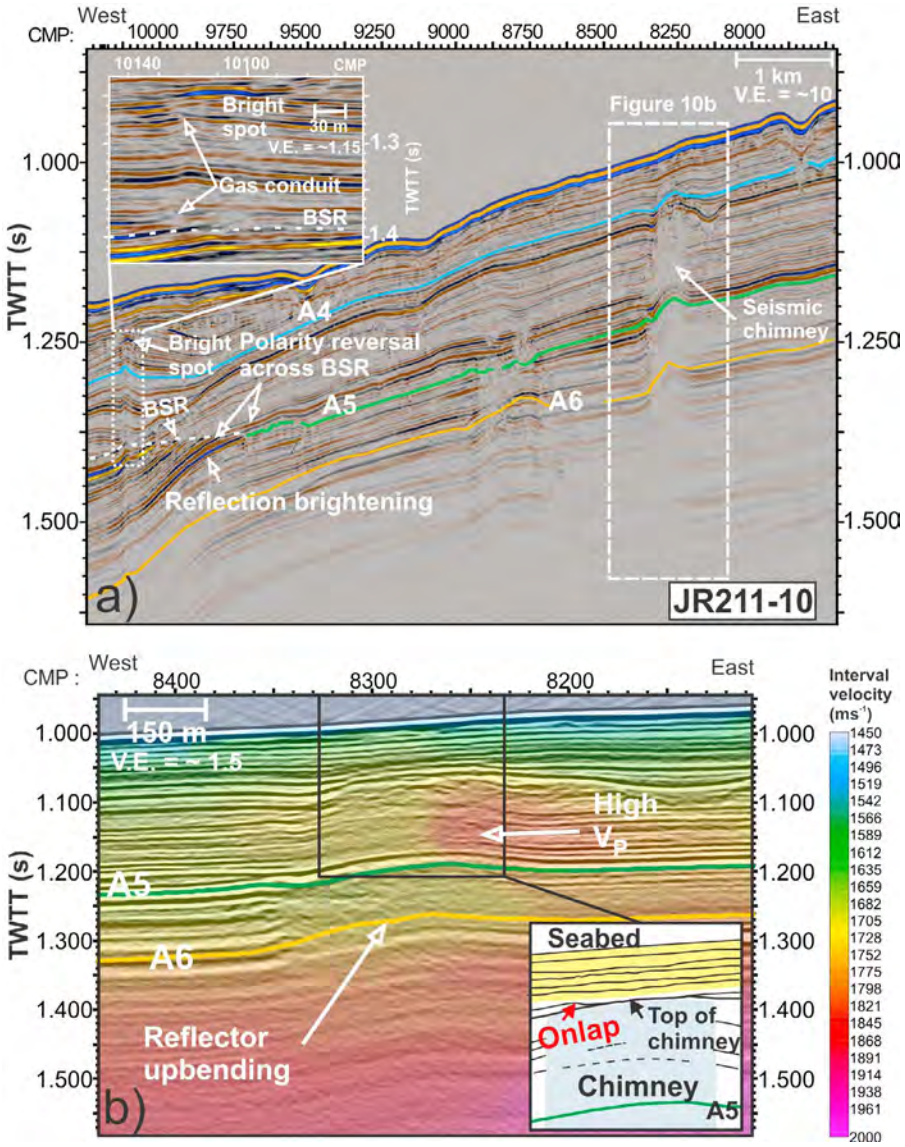

Figure 10. Seismic line JR211-10 shows a BSR and seismic chimney. (a) A BSR parallels the seafloor and crosscuts strata beneath the mid slope. Polarity reversal is observed across the BSR and reflection brightening below it. A vertical seismic chimney is observed beneath the upper slope (near CMP 8250). The chimney shows suppressed amplitude and reflector upbending. Another gas migration conduit is seen within the GHSZ near CMP 10125 and it terminates in a bright spot with reversed polarity. (b) A localized area of relatively high interval velocity within the chimney (chimney location in Figure 10a) probably indicates presence of hydrate. Reflector onlap on top of the chimney is shown in an inset.

with its base at ~645 m depth. The overlying well-stratified parallel-bedded reflectors with gentle down-warping geometry (probably mimicking the depression caused by the deeper channel) also show low V_P. Several shallow low velocity anomalies occur in pockets below the gas seepage sites and close to the seafloor, beneath the upper slope (Figure 12a) and the shelf break (Figure 12d).

4.4. Modeling the Base of Methane Hydrate Stability

[23] We identify a BSR in the inter-fan region at water depths >600 m but it is not found at shallower depth and below the gas seepage sites (Figure 2). In absence of a BSR as the direct seismic evidence for the base of methane hydrate stability (BMHS) beneath the uppermost continental slope, modeling is used to predict the BMHS. The modeling allows the probable zone of hydrate dissociation associated with bottom water warming to be estimated. We use the phase boundary for pure methane hydrate in seawater (salinity 35‰) derived by *Moridis* [2003] and assume hydrostatic pressure. The curve defining the BMHS in the upper part of the continental slope is not unique, because of uncertainties associated with bottom water temperature and variations of geothermal gradient. We estimate a BSR derived geothermal gradient based on the method established by *Yamano et al.* [1982] (Figures S3 and S4 in the auxiliary material). Based on the observed variation of inferred geothermal gradient with water depth as the sediment cover thickens and the distance from the mid-oceanic ridge

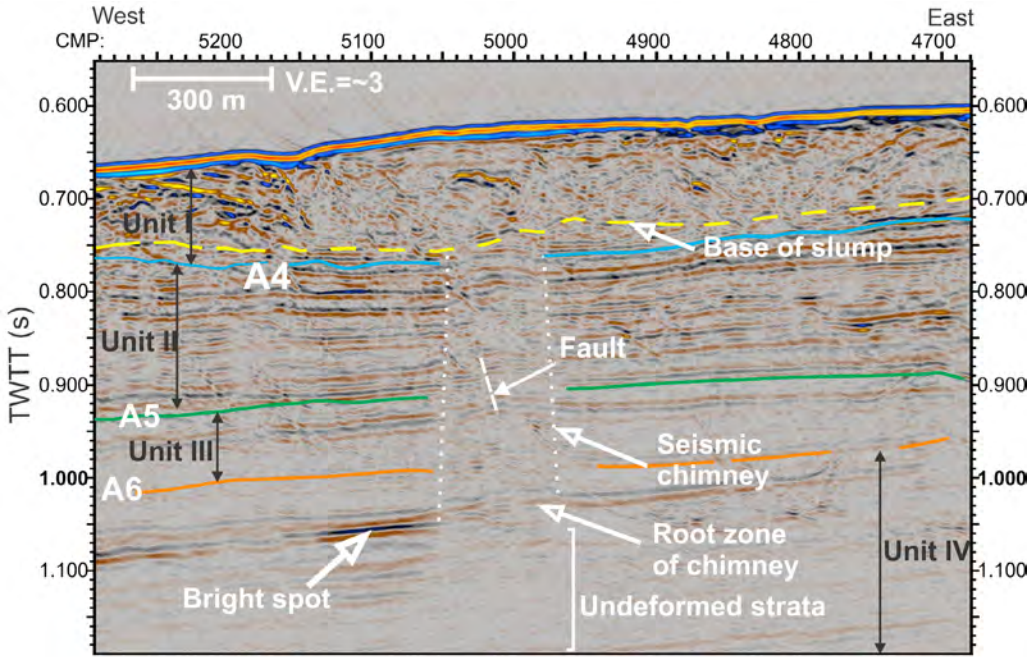

Figure 11. A seismic chimney in profile JR211-10 located on the upper slope (Profile location in Figure 3a). The chimney shows internal weak amplitude and terminates in a slump deposit.

increases, we estimate a geothermal gradient of 53–61°C/km at the gas seepage site (water depth ~400 m, Figure S5 in the auxiliary material).

[24] In order to observe the resulting variations in the MHSZ thickness at the upper continental slope, we overlay the resulting BMHS curves (considering a range of geothermal gradient 50–70°C/km with an increment of 10°C/km and bottom water temperatures of 2° and 3°C) on the seismic section (Figure S6 in the auxiliary material). The probable zone of hydrate dissociation lies between the BMHS curves predicted for 2° and 3°C bottom water temperatures assuming the temperature change has reached the BMHS. Based on *Moridis*'s [2003] pure methane hydrate stability curve with seawater salinity, a water depth of 373 m corresponds to the landward limit of the BMHS at 2°C bottom water temperature, whereas the limit lies at greater depth (412 m) for 3°C bottom water temperature. For the rest of the paper we consider 370 m and 410 m (Figure 13a) as reference values for this limit at 2°C and 3°C bottom water temperatures respectively.

5. Discussion

[25] The gas seepage area shows a linear trend and mostly follows the bathymetric contours (confined between 370 and 410 m depths in the uppermost slope, Figure 2). This depth range corresponds to the area over which the BMHS retreated in response to bottom water warming by 1°C (i.e., from a depth of 370 m at 2°C to a depth of 410 m at 3°C). Therefore, gas hydrate dissociation is a plausible explanation for the gas seeps [*Westbrook et al.*, 2009]. However, the gas seeps in the northern inter-fan area occur at shallower depth (230–250 m) close to the shelf break and not within the predicted hydrate retreat area. Here we discuss the subseabed occurrences of gas and examine alternative processes that can focus gas to the seabed in a narrow zone, in addition to the possible role of hydrate dissociation.

5.1. Indications of Deep and Shallow Gas Occurrence

[26] Bright spots with reversed polarity commonly indicate accumulations of free gas [e.g., *Judd and Hovland*, 1992]. We find gas accumulations at the crests of sediment waves (Figure 4a) and within the well-stratified, parallel-bedded marine sedimentary package of Unit IV beneath the slope and shelf (Figure 3a). The crests of sediment waves are probably composed of well-sorted marine sediments and hence they can store appreciable amounts of fluid. Within the shallow glacimarine sediments of Unit I, gas occurs beneath both the upper continental slope and the outer shelf (Figures 7, 8 and 9). Reflection brightening below and adjacent to channels (Figure 9) indicates that gas is trapped at the bases and sides of channels filled with less permeable, clay rich glacigenic sediments.

5.2. Gas Venting Through Ploughmarks

[27] Numerous seafloor iceberg ploughmarks in 300–600 m water depth in the inter-fan area (Figure 5) are scattered over a region with shallow gas pockets occurring at depth <75 m below the seafloor (e.g., Figures 8 and 9), and apparently have an effect on gas migration. Beneath the ploughmarks, cracks and fissures, induced by iceberg movement, may locally promote gas migration close to the seabed [*Hovland and Judd*, 1988]. Amplitude fading and a bright spot at the base of a ploughmark (Figure 6) indicates that gas has accumulated below that ploughmark, but there is no evidence for seafloor gas seepage from this ploughmark. Gas seeps and ploughmarks are rarely co-located. Ploughmarks might have locally influenced shallow gas focusing to the seabed (Figure 5, Inset 1), but there is no evidence for gas seeps from ploughmarks outside the area in which hydrate

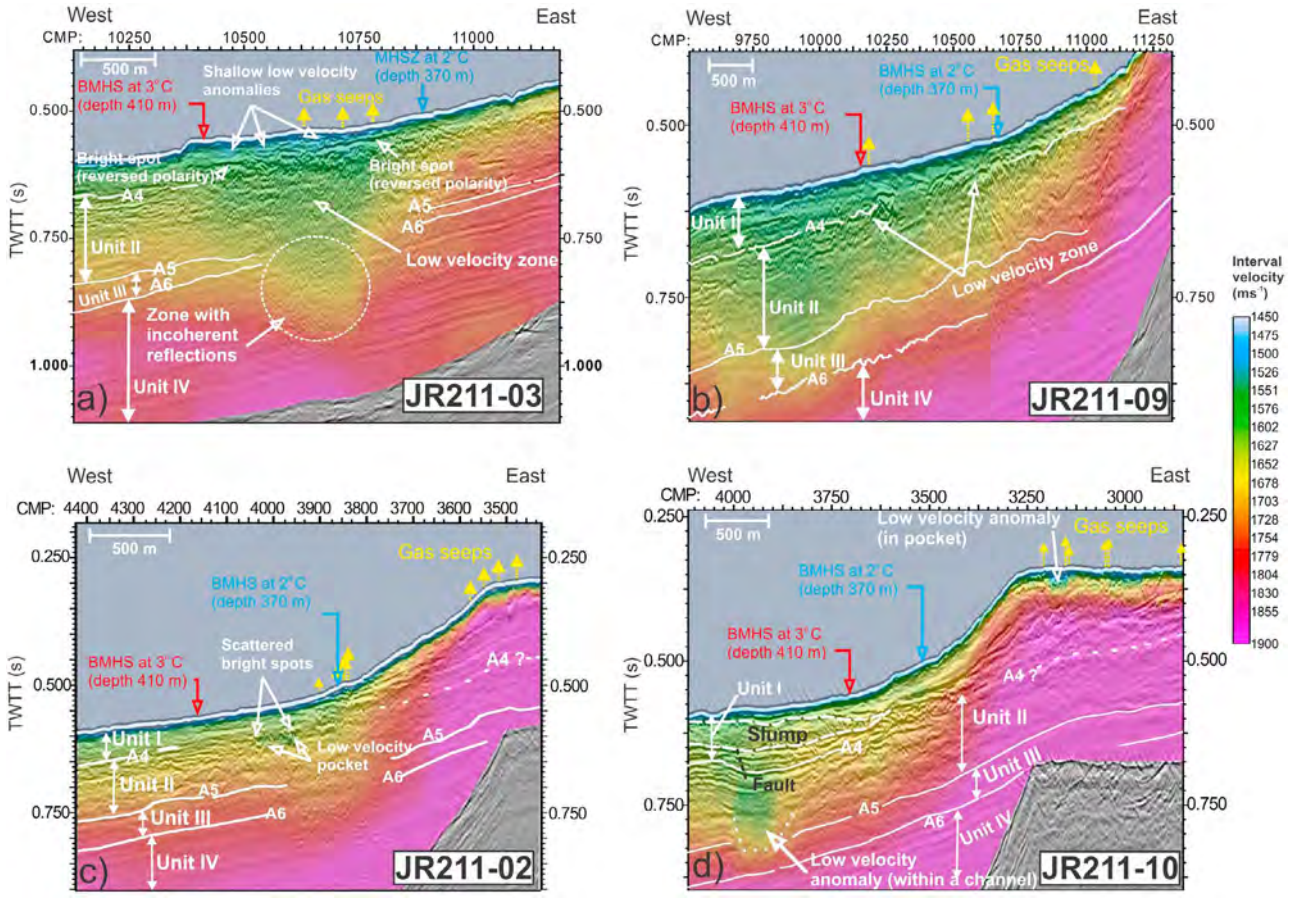

Figure 12. Interval velocity superimposed on seismic sections showing velocity variations beneath the upper continental slope. (a) Profile JR211-03 (location in Figure 4a) showing a broad low-velocity zone that extends down to Unit IV. Several shallow low-velocity anomalies are confined between the seafloor and the bright spots within Unit I. (b) Profile JR211-09 (location in Figure 2) showing a low-velocity anomaly under water depth 0.52–0.60 s TWTT (~385–435 m). (c) Profile JR211-02 (location in Figure 2) shows low-velocity pockets that coincide with scattered bright spots with reversed polarity at the base of Unit I. (d) Profile JR211-10 (location in Figure 3a) showing a low-velocity zone within a channel and overlying stratified reflectors of Unit II. Shallow low-velocity pockets occur beneath the gas seepage sites on the shelf.

dissociation due to bottom water warming is postulated. Moreover, the ploughmarks have a wide range of orientations and cannot explain the well-defined trend of the seafloor gas seeps.

5.3. Vertical/Near-Vertical Gas Migration System

[28] Seismic chimneys showing vertical zones of reduced amplitude represent conduits that focus fluid flow from depth to shallower levels [*Heggland*, 1997]. We do not observe any seismic chimneys that terminate at the seafloor on the uppermost slope (300–400 m water depths). However, we observe a chimney below the slump deposit (water depth 450 m) in the northern inter-fan region (Figure 11). It is rooted below horizon A6 and at the stratigraphic level of a gas pocket. Small-scale faults are present inside it, but do not offset the reflections below the chimney. We attribute its origin to a local deformation process perhaps induced by loading of the sediments during deposition of the overlying slump. Chimneys in deeper water (>depth 700 m) are buried (Figure 10a), such as a chimney near CMP 8250 in Figures 10a and 10b. This chimney shows up-bending of reflectors with almost the same amount of up-bending throughout, a localized high velocity anomaly that results in negligible velocity pull-up (3 ms) compared with the pronounced up-bending (30 ms) in the center, and positive relief at the top with no overlying high velocity. It appears to be the result of deformation associated with fluid migration. In deeper water we find evidence for gas migration, such as a near-vertical zone of amplitude fading and a bright spot at its top (near CMP 10120, Figure 10a, inset). This feature does not resemble a typical chimney in the 2D profile and we identify it more generally as a gas conduit. We suggest that gas migrates through the GHSZ, but does not vent to the seafloor. Hydrate and gas can co-exist in the GHSZ, if hydrate formation is slowed down by a lack of water (removed by hydrate formation) or by an increase of pore water salinity due to the expulsion of chloride from hydrate [*Liu and Flemings*, 2007].

[29] Gas migration through faults is a possible explanation for the gas seeps. Minor faults (below water depth 420 m)

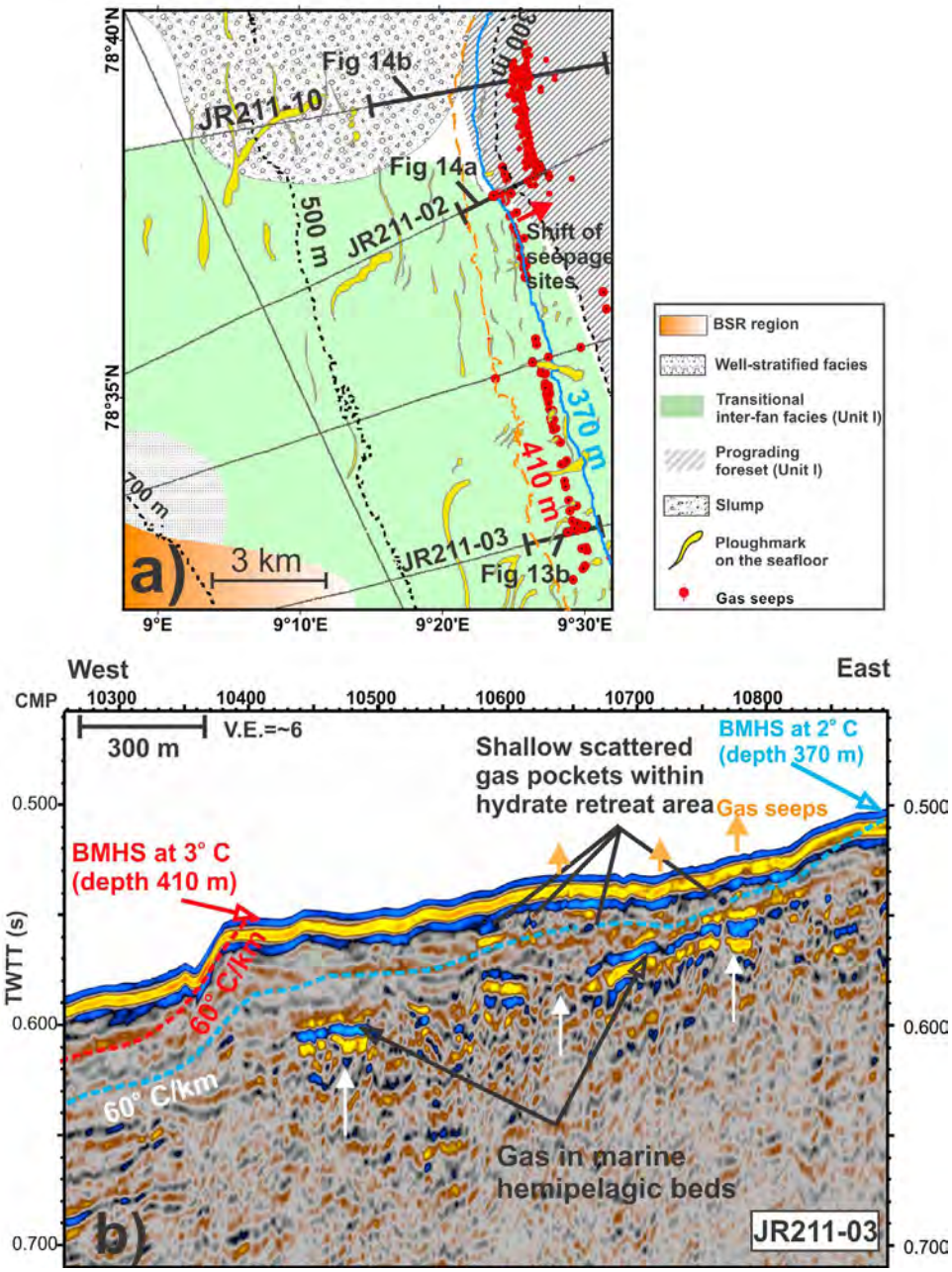

Figure 13. (a) Overview map of the inter-fan area showing the distribution of seismic facies in Unit I, ploughmarks on the seafloor and location of the gas seeps. The hydrate retreat area on the seafloor, caused by 1°C bottom water temperature rise (from 2° to 3°C), is confined between 370 and 410 m depths. The gas seepage locations shift from the upper slope to the shelf break in the north. The shift coincides with a transition from prograding foreset facies in the distal shelf to transitional inter-fan facies in the upper slope. (b) Seismic profile JR211-03 (profile location in Figure 13a) showing shallow bright spots below the modeled BMHS (2°C bottom water temperature) and scattered gas pockets within the predicted hydrate retreat area. Near-vertical gas migration through fractures is marked by white arrows.

are locally present below the slump in the northern inter-fan region (Figure 3a, Inset 1 and Figure 12d). Gas-charged horizons are juxtaposed against a fault below the slump (profile JR211–10, Figure 3a, Inset 1) and the low-V_P anomaly around the faulted strata (profile JR211–10, Figure 12d) indicates the presence of gas. Except for this example, we do not observe any fault that originates at depth and passes through or terminates at the low-velocity zones within the shallow glacimarine strata of Units I–III in the upper slope (Figures 12a and 12b) and below the gas seepage sites. Therefore, gas migration along faults is not a viable explanation for the gas seeps.

[30] Vertical/near-vertical gas migration below the gas seepage area (water depths 300–400 m; e.g., Figure 8) in the

uppermost continental slope of the inter-fan region is represented by a zone with scattered reflections indicating gas rising up through fractures within glacigenic strata (Figure 8, Inset 1 and Figure 7, Inset 2). A low-velocity anomaly (Figure 12a) within the shallow scattered reflection zone (Figure 10a) also indicates the presence of gas. However, the apparently deeper scattered reflections within Units III and IV (Figure 8) are from out-of-plane occurrences of gas at shallower depth. Gas rising through fractures locally feeds the dipping marine hemipelagic beds in Unit I below the upper continental slope (water depths 300–400 m, Figure 13b).

5.4. Lateral Gas Migration

[31] Interbedded marine hemipelagic and glacigenic strata constitute the transitional inter-fan facies of Units I–II. Within this facies several shallow gas pockets occur along seaward dipping marine beds (dip 1.5 degree westerly, Figure 13b) below the uppermost continental slope (water depths 350–700 m). The hemipelagic interbeds are more porous (as they are well-sorted) and permeable than the glacigenic strata, so, they can store and transmit appreciable amounts of gas. In the northern inter-fan area, there is a deviation of the locations of gas seeps from the probable hydrate retreat area on the upper slope to the shelf break (Figures 2 and 13a). This area is located at the facies transition between transitional inter-fan facies and prograding foreset within Unit I (Figure 13a). Gas hydrate dissociation is not the direct cause of the presence of gas here, as this location lies outside the predicted MHSZ. Here gas rising up through fractures gets steered by the prograding foresets toward the shelf break, as indicated by gas pockets (Figure 14a) at several places along foreset reflectors (e.g., reflector F, Figure 7). Further north in the inter-fan area, the slump may inhibit rising of gas and formation of gas hydrate close to the seafloor (Figure 14b).

5.5. Role of Gas Hydrate Dissociation

[32] We could not generally identify the BSR in water depths shallower than about 700 m, although it does occur locally in a water depth of 580 m of the upper continental slope. The absence of the BSR does not rule out the presence of hydrate and hydrate may be present at low saturations [*Chabert et al.*, 2011]. Moreover, the wavelet from seabed reflection is 12 ms TWTT long (10 m distance) and masks any reflection arising from free gas or BSR in the top 10 m below the seafloor. A supply of free gas is essential for hydrate formation within the hydrate stability zone. We find evidence for free gas immediately below (5–15 m) the BMHS predicted for 2°C bottom water temperature (Figure 13b), where gas flow through near-vertical fractures and dipping marine beds significantly enhance supply of gas. From there gas might have migrated through fractures or permeable marine beds into the zone of hydrate stability and formed gas hydrates when conditions were cooler than at present.

[33] Time series measurements of ocean temperature along the route of the North Atlantic Current from the Subpolar Gyre to the Fram Strait reveal a cooling trend in the northern North Atlantic that preceded the warming seen after 1980s [*Holliday et al.*, 2008]. For example, the upper ocean in the southern Norwegian Sea decreased in temperature by about 1°C, over the period 1960 to 1980. Although the record from west of Spitsbergen is limited before the 1970s, the correlation between temperature variation in the southern Norwegian Sea and offshore Spitsbergen observed since then [*Holliday et al.*, 2008] indicates that this cooling also occurred off Spitsbergen. During this cooling episode, hydrate probably formed within the shallow uppermost continental slope before this region was moved out of the hydrate stability during more recent warming.

[34] To examine whether gas seeps can emerge after 30 years from the onset of long-term warming, the time delays associated with thermal diffusion, hydrate dissociation and gas migration from the sites of dissociation to the seabed need to be considered. *Reagan and Moridis* [2009] and *Thatcher and Westbrook* [2011] have modeled the time-dependent evolution of the GHSZ in response to warming. For annual variation, the duration of warming may not be sufficient for complete hydrate dissociation (as the process is endothermic), even if the top of the hydrate is only 1 m below the seabed, and almost all the gas released by dissociation reforms hydrate as temperature decreases again, rather than escaping through to seabed. A model simulation adapted to conditions west of Svalbard shows that observed bottom water temperature variations during 1975–2008 can lead to gas release at the seabed by 2008 if hydrate (a 7 m thick hydrate layer at 5% saturation) occurs at a depth of 5 m below the seabed (a factor that controls this depth is the sulfate reduction zone, which limits the presence of hydrate near the seabed) and fractures increase the effective permeability above that typical of glacigenic sediments [*Thatcher and Westbrook*, 2011]. Such enhancement of permeability is realistic given the seismic evidence for gas flow through fractures within glacigenic sediments in the upper continental slope (Figure 13b). Therefore, both numerical modeling and the seismic evidence support a contribution from hydrate dissociation to the gas seeps.

[35] Another potential mechanism for focusing gas to the landward edge of the BMHS is lateral gas migration along the BMHS [*Crutchley et al.*, 2010]. However, in the upper continental slope (400–700 m water depth), the positions of the scattered gas pockets just below the predicted BMHS (for 2°C bottom water temperature, Figure 13b) appear to be controlled by lithology. The poorly stratified, low-permeability glacigenic sediments, which are abundantly present here, appear not to contain large enough sedimentary units with high enough porosity to develop a gas layer that has sufficient lateral extent to produce reflector that can be distinguished from the surrounding reflectors representing lithological boundaries. So although, in general, free gas is excluded from the MHSZ, the migration of gas outside the GHSZ exploits the heterogeneity of lithology-dependent permeability and, for this reason, there is no BSR following the BMHS with any noticeable continuity in this part of the slope.

[36] The shallowest gas pockets within the probable hydrate retreat area (the area bounded by the BMHS curves for bottom water temperatures of 2°C and 3°C) are observed at depths 15–25 m below the seabed (Figure 13b). Most of them are in the vicinity of the seabed seeps. This shallow gas may be the product of gas hydrate dissociation and the observed gas seeps may result from venting of this gas as predicted by modeling. As most of the gas pockets occur above areas of gas flow through gas-bearing marine strata, the gas that formed the hydrate is most likely to be gas that

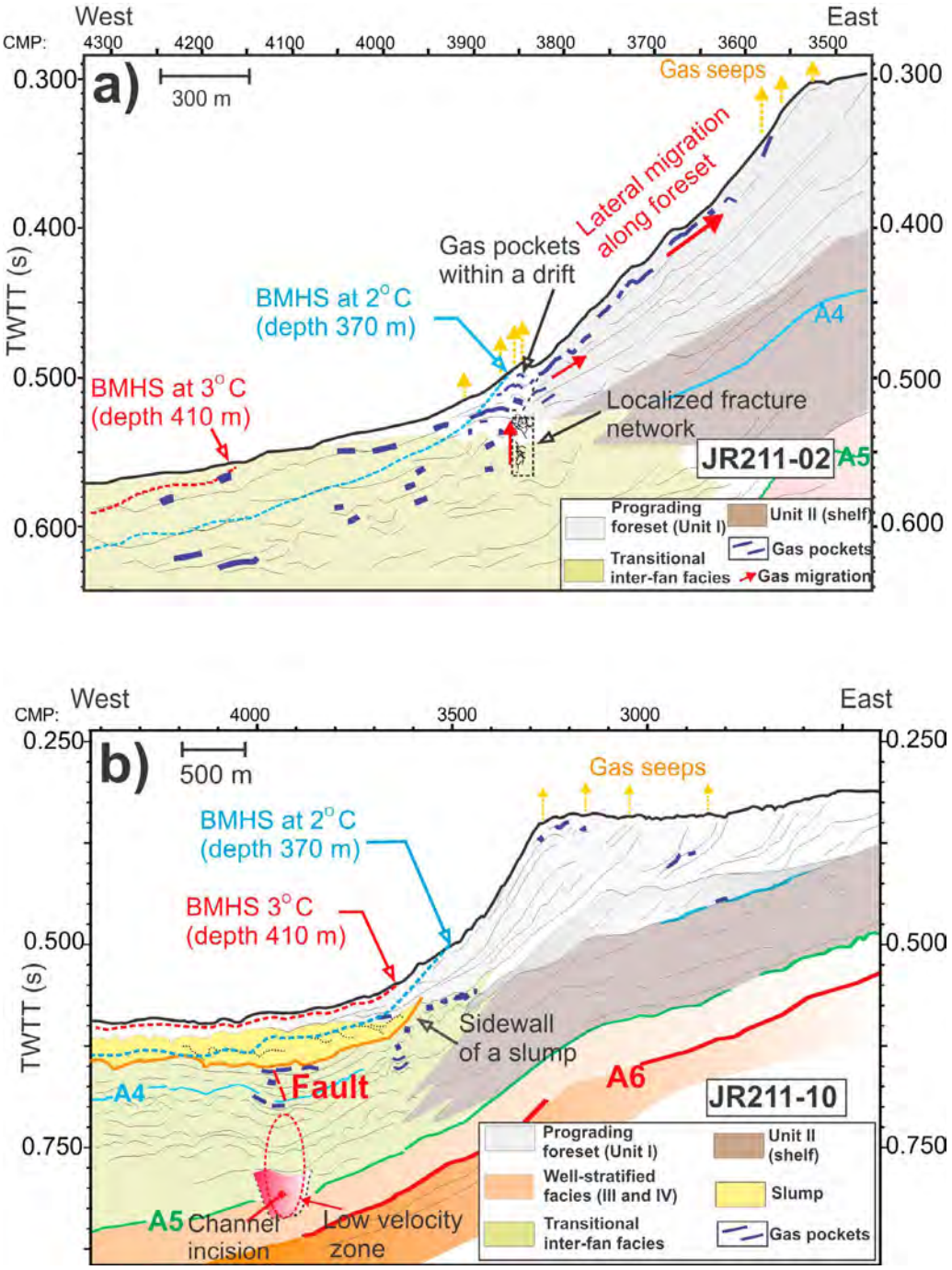

Figure 14. (a) Line drawing (location in Figure 13a) and interpretation of profile JR211-02 (based on Figure 7). Gas seeps are located near the toe of prograding foreset within Unit I and close to a drift mound. Gas migrates updip along the foreset toward the shelf break. (b) Line drawing of JR211-10 (location Figure 13a) based on interpretations shown in Figures 3a, 3b and 12d. A shallow buried slump within Unit I hinders vertical gas migration as gas is mostly trapped at the base of the slump.

migrated up the continental slope and moved close to the seabed through fractures and hemipelagic interbeds in the glacigenic sediments. Although occurrence of gas seeps in a narrow range of water depths (370–410 m) from which the MHSZ is postulated to have retreated over the last 33 years, can be explained by warming-induced gas hydrate dissociation, the scatter of individual gas seepage locations within this depth range is probably a consequence of lithologically controlled focusing of gas close to the seabed at the sites of hydrate formation, or release of gas once hydrate dissociated. Therefore, based on (a) the presence of gas pockets within the probable hydrate retreat area, (b) the rarity of gas seeps downslope of the present-day BMHS (3°C bottom water temperature), probably indicating the retention of methane as hydrate and permeability reduction caused by hydrate within the GHSZ, (c) evidence for the supply of gas

through fractures and marine beds to the area where hydrate might have formed prior to the onset of recent warming and (d) modeling results that can explain methane emission from dissociating hydrate in a time scale of three decades in response to observed bottom water warming [*Thatcher and Westbrook*, 2011], we infer that hydrate dissociation is likely to contribute most or all of the gas that is venting from the seabed, although the absence of the GHSZ from the retreat area will enable gas migrating up the continental slope to flow directly to the seabed without being intercepted by the GHSZ.

6. Conclusions

[37] Seismic evidence, in the form of negative-polarity bright spots, localized zones of low velocity, seismic attenuation and scattering, indicates gas occurrence in the uppermost continental slope below the gas seepage sites. The gas occurs in shallow pockets located below the predicted BMHS beneath the upper slope. We infer that the gas has migrated to these pockets through permeable glacimarine strata and fractures, although individual fractures are too small to be imaged in our data. The widespread presence of a BSR in water depths greater than 700 m and numerous seismic indicators of the presence of free gas in the deeper strata throughout the continental slope, indicate that gas migration from the thick marine sedimentary section contributes most, if not all, of the gas emitted by seeps in the uppermost part of the slope.

[38] A BSR is present beneath the seabed in deeper water (depths >600 m), but it has not been observed below shallower water (400–600 m) in which the GHSZ has been predicted to occur. There is no clear evidence of unimpeded migration of gas along the BMHS. Gas pockets are scattered in shallow glacimarine strata below the modeled BMHS and it appears that the effect of permeability reduction caused by hydrate within the GHSZ is secondary to the effect of lithology in controlling the flow of gas.

[39] Several observations indicate that hydrate dissociation can be the primary cause of the gas seeps on this part of the west Svalbard upper continental slope. The gas seeps come mainly from the seabed of the predicted zone of GHSZ retreat caused by bottom water warming. Within this zone, there are low seismic-velocity anomalies and negative-polarity seismic bright spots, indicating the presence of free gas. These features are generally absent from the GHSZ where it is predicted to exist, downslope. Gas migrating into what is now the GHSZ retreat zone from beneath the GHSZ or elsewhere 30 years or more ago, when the seabed was 1°C cooler, would have formed hydrate. Modeling shows that some of the gas released by the dissociation of that hydrate will still exist and not yet have been completely replaced by gas migrating into the zone since the hydrate dissociated. The absence of seismic evidence for faults below the gas seepage sites excludes the possibility that faults guide gas from deeper gas-rich strata directly to the locations of the seeps.

[40] Gas seeps are absent in the north where a slump deposit occurs close to the seabed. The slump deposit probably hinders vertical gas migration or hydrate formation close to the seafloor. Numerous seeps at the shelf break in the northern inter-fan region are a result of lateral gas migration upslope, along prograding foreset beds.

[41] Most of the uppermost continental slope of the inter-fan area (water depths 300–600 m) contains shallow sedimentary features, such as channels and interbedding of more permeable marine sedimentary units with units of less permeable glacigenic sediments, that introduce a high degree of heterogeneity in the lithology and permeability of sedimentary units, strongly affecting shallow gas migration. This heterogeneity will have influenced the locations of gas seeps as much by controlling the locations where hydrate formed within the sediment as by determining the migration paths of gas released from hydrate dissociation.

[42] **Acknowledgments.** This work was supported by the Natural Environment Research Council as a part of the International Polar Year 2007–2008 (grant number NE/D005728). The captain and crew of RRS James Clark Ross provided essential support for the acquisition of the data during the JR211 cruise. We thank the Aarhus University for lending us their streamer. Part of the bathymetric image shown in Figure 2 was derived from the data provided by the Norwegian Hydrographic Service (NHS). S. Sarkar is grateful to Inlaks Shivdasani Foundation, India and the Graduate School of the National Oceanography Centre, Southampton, UK for the financial support of his PhD studies. We thank the Associate Editor, two anonymous reviewers and Ingo Pecher for constructive comments.

References

Bass, D. W., and C. Woodworth-Lynas (1988), Iceberg crater marks on the sea floor, Labrador Shelf, *Mar. Geol.*, *79*(3–4), 243–260, doi:10.1016/0025-3227(88)90041-2.

Bellec, V., M. Wilson, R. Boe, L. Rise, T. Thorsnes, L. Buhl-Mortensen, and P. Buhl-Mortensen (2008), Bottom currents interpreted from iceberg ploughmarks revealed by multibeam data at Tromsøflaket, Barents Sea, *Mar. Geol.*, *249*(3–4), 257–270, doi:10.1016/j.margeo.2007.11.009.

Biastoch, A., et al. (2011), Rising Arctic Ocean temperatures cause gas hydrate destabilization and ocean acidification, *Geophys. Res. Lett.*, *38*, L08602, doi:10.1029/2011GL047222.

Chabert, A., T. A. Minshull, G. K. Westbrook, C. Berndt, K. E. Thatcher, and S. Sarkar (2011), Characterization of a stratigraphically constrained gas hydrate system along the western continental margin of Svalbard from ocean bottom seismometer data, *J. Geophys. Res.*, *116*, B12102, doi:10.1029/2011JB008211.

Comiso, J. C., C. L. Parkinson, R. Gersten, and L. Stock (2008), Accelerated decline in the Arctic Sea ice cover, *Geophys. Res. Lett.*, *35*, L01703, doi:10.1029/2007GL031972.

Crutchley, G., I. A. Pecher, A. R. Gorman, S. Henrys, and J. Greinert (2010), Seismic imaging of gas conduits beneath seafloor vent sites in a shallow marine gas hydrate province, Hikurangi Margin, New Zealand, *Mar. Geol.*, *272*(1–4), 114–126, doi:10.1016/j.margeo.2009.03.007.

Dowdeswell, J. A., and A. Elverhøi (2002), The timing of initiation of fast-flowing ice streams during a glacial cycle inferred from glacimarine sedimentation, *Mar. Geol.*, *188*(1–2), 3–14, doi:10.1016/S0025-3227(02)00272-4.

Eiken, O., and K. Hinz (1993), Contourites in the Fram Strait, *Sediment. Geol.*, *82*(1–4), 15–32, doi:10.1016/0037-0738(93)90110-Q.

Engen, Ø., J. I. Faleide, and T. K. Dyreng (2008), Opening of the Fram Strait gateway: A review of plate tectonic constraints, *Tectonophysics*, *450*(1–4), 51–69, doi:10.1016/j.tecto.2008.01.002.

Fisher, R. E., et al. (2011), Arctic methane sources: Isotopic evidence for atmospheric inputs, *Geophys. Res. Lett.*, *38*, L21803, doi:10.1029/2011GL049319.

Frantzen, J. H. P. (2008), Fluid-flow expressions at Vestnesa Ridge of the NW-Svalbard Margin, MS thesis, Dep. of Geol., Univ. of Tromsø, Tromsø, Norway.

Haacke, R. R., R. D. Hyndman, K. P. Park, D. G. Yoo, I. Stoian, and U. Schmidt (2009), Migration and venting of deep gases into the ocean through hydrate-choked chimneys offshore Korea, *Geology*, *37*(6), 531–534, doi:10.1130/G25681A.1.

Heggland, R. (1997), Detection of gas migration from a deep source by the use of exploration 3D seismic data, *Mar. Geol.*, *137*(1–2), 41–47, doi:10.1016/S0025-3227(96)00077-1.

Hester, K. C., and P. G. Brewer (2009), Clathrate hydrates in nature, *Annu. Rev. Mar. Sci.*, *1*, 303–327, doi:10.1146/annurev.marine.010908.163824.

Hohbein, M., and J. Cartwright (2006), 3D seismic analysis of the West Shetland Drift system: Implications for Late Neogene palaeoceanography

of the NE Atlantic, *Mar. Geol.*, *230*(1–2), 1–20, doi:10.1016/j.margeo.2006.03.009.

Holliday, N. P., et al. (2008), Reversal of the 1960s to 1990s freshening trend in the northeast North Atlantic and Nordic Seas, *Geophys. Res. Lett.*, *35*, L03614, doi:10.1029/2007GL032675.

Houghton, J. T., Y. Ding, D. J. Griggs, M. Noguer, P. J. van der Linden, X. Dai, K. Maskell, and C. A. Johnson (Eds.) (2001), *Climate Change 2001: The Scientific Basis*, 881 pp., Cambridge Univ. Press, Cambridge, U. K.

Hovland, M., and J. Judd (1988), *Seabed Pockmarks and Seepages: Impact on Geology, Biology and Marine Environment*, 293 pp., Graham and Trorman, London.

Howe, J. A., T. M. Shimmield, and R. Harland (2008), Late Quaternary contourites and glaciomarine sedimentation in the Fram Strait, *Sedimentology*, *55*(1), 179–200, doi:10.1111/j.1365-3091.2007.00897.x.

Hustoft, S., S. Bünz, J. Mienert, and S. Chand (2009), Gas hydrate reservoir and active methane-venting province in sediments on <20 Ma young oceanic crust in the Fram Strait, offshore NW-Svalbard, *Earth Planet. Sci. Lett.*, *284*(1–2), 12–24, doi:10.1016/j.epsl.2009.03.038.

Isaksen, I. S. A., M. Gauss, G. Myhre, K. M. W. Anthony, and C. Ruppel (2011), Strong atmospheric chemistry feedback to climate warming from Arctic methane emissions, *Global Biogeochem. Cycles*, *25*, GB2002, doi:10.1029/2010GB003845.

Jakobsson, M., R. Macnab, L. Mayer, R. Anderson, M. Edwards, J. Hatzky, H. W. Schenke, and P. Johnson (2008), An improved bathymetric portrayal of the Arctic Ocean: Implications for ocean modeling and geological, geophysical and oceanographic analyses, *Geophys. Res. Lett.*, *35*, L07602, doi:10.1029/2008GL033520.

Judd, A. G., and M. Hovland (1992), The evidence of shallow gas in marine sediments, *Cont. Shelf Res.*, *12*(10), 1081–1095, doi:10.1016/0278-4343(92)90070-Z.

Knies, J., J. Matthiessen, C. Vogt, J. S. Laberg, B. O. Hjelstuen, M. Smelror, E. Larsen, K. Andreassen, T. Eidvin, and T. O. Vorren (2009), The Plio-Pleistocene glaciation of the Barents Sea-Svalbard region: A new model based on revised chronostratigraphy, *Quat. Sci. Rev.*, *28*(9–10), 812–829, doi:10.1016/j.quascirev.2008.12.002.

Kvenvolden, K. A. (1993), Gas hydrates—Geological perspective and global change, *Rev. Geophys.*, *31*(2), 173–187, doi:10.1029/93RG00268.

Kvenvolden, K. A., G. D. Ginsburg, and V. A. Soloviev (1993), Worldwide distribution of subaquatic gas hydrates, *Geo Mar. Lett.*, *13*(1), 32–40, doi:10.1007/BF01204390.

Liu, X., and P. B. Flemings (2007), Dynamic multiphase flow model of hydrate formation in marine sediments, *J. Geophys. Res.*, *112*, B03101, doi:10.1029/2005JB004227.

Moridis, G. J. (2003), Numerical studies of gas production from methane hydrates, *SPE J.*, *8*(4), 359–370, doi:10.2118/87330-PA.

Ottesen, D., J. A. Dowdeswell, J. Y. Landvik, and J. Mienert (2007), Dynamics of the Late Weichselian ice sheet on Svalbard inferred from high-resolution sea-floor morphology, *Boreas*, *36*(3), 286–306, doi:10.1111/j.1502-3885.2007.tb01251.x.

Petersen, C. J., S. Bünz, S. Huston, J. Mienert, and D. Klaeschen (2010), High-resolution P-Cable 3D seismic imaging of gas chimney structures in gas hydrated sediments of an Arctic sediment drift, *Mar. Pet. Geol.*, *27*(9), 1981–1994, doi:10.1016/j.marpetgeo.2010.06.006.

Piechura, J., and W. Walczowski (2009), Warming of the West Spitsbergen Current and sea ice north of Svalbard, *Oceanologia*, *51*(2), 147–164, doi:10.5697/oc.51-2.147.

Posewang, J., and J. Mienert (1999), High-resolution seismic studies of gas hydrates west of Svalbard, *Geo Mar. Lett.*, *19*(1–2), 150–156, doi:10.1007/s003670050102.

Reagan, M. T., and G. J. Moridis (2009), Large-scale simulation of methane hydrate dissociation along the West Spitsbergen Margin, *Geophys. Res. Lett.*, *36*, L23612, doi:10.1029/2009GL041332.

Sarkar, S., C. Berndt, A. Chabert, D. G. Masson, T. A. Minshull, and G. K. Westbrook (2011), Switching of a paleo-ice stream in northwest Svalbard, *Quat. Sci. Rev.*, *30*(13–14), 1710–1725, doi:10.1016/j.quascirev.2011.03.013.

Schauer, U., A. Beszczynska-Möller, W. Walczowski, E. Fahrbach, J. Piechura, and E. Hansen (2008), Variation of measured heat flow through the Fram Strait Between 1997 and 2006, in *Arctic–Subarctic Ocean Fluxes*, edited by R. Dickson, J. Meincke, and P. Rhines, pp. 65–85, Springer, Dordrecht, Netherlands, doi:10.1007/978-1-4020-6774-7_4.

Shipley, T. H., M. H. Houston, R. T. Buffler, F. J. Shaub, K. J. McMillen, J. W. Ladd, and J. L. Worzel (1979), Seismic evidence for widespread possible gas hydrate horizons on continental slopes and rises, *AAPG Bull.*, *63*(12), 2204–2213.

Solheim, A., E. S. Andersen, A. Elverhøi, and A. Fiedler (1996), Late Cenozoic depositional history of the western Svalbard continental shelf, controlled by subsidence and climate, *Global Planet. Change*, *12*(1–4), 135–148, doi:10.1016/0921-8181(95)00016-X.

Spielhagen, R. F., K. Werner, S. A. Sorensen, K. Zamelczyk, E. Kandiano, G. Budeus, K. Husum, T. M. Marchitto, and M. Hald (2011), Enhanced modern heat transfer to the Arctic by warm Atlantic Water, *Science*, *331*(6016), 450–453, doi:10.1126/science.1197397.

Stoll, R. D., and G. M. Bryan (1979), Physical properties of sediments containing gas hydrates, *J. Geophys. Res.*, *84*(B4), 1629–1634, doi:10.1029/JB084iB04p01629.

Thatcher, K., and G. K. Westbrook (2011), Timing of methane release from hydrate dissociation on the west Svalbard margin, paper presented at 7th International Conference on Gas Hydrates, Edinburgh, U. K., 17–23 July 2011.

Vanneste, M., S. Guidard, and J. Mienert (2005), Bottom-simulating reflections and geothermal gradients across the western Svalbard margin, *Terra Nova*, *17*(6), 510–516, doi:10.1111/j.1365-3121.2005.00643.x.

Vanneste, M., C. Berndt, J. S. Laberg, and J. Mienert (2007), On the origin of large shelf embayments on glaciated margins—Effects of lateral ice flux variations and glacio-dynamics west of Svalbard, *Quat. Sci. Rev.*, *26*(19–21), 2406–2419, doi:10.1016/j.quascirev.2007.05.005.

Vogt, P. R., K. Crane, E. Sundvor, M. D. Max, and S. L. Pfirman (1994), Methane-generated (?) pockmarks on young, thickly sedimented oceanic-crust in the Arctic: Vestnesa ridge, Fram Strait, *Geology*, *22*(3), 255–258, doi:10.1130/0091-7613(1994)022<0255:MGPOYT>2.3.CO;2.

Vorren, T. O., and J. S. Laberg (1997), Trough mouth fans—Palaeoclimate and ice-sheet monitors, *Quat. Sci. Rev.*, *16*(8), 865–881, doi:10.1016/S0277-3791(97)00003-6.

Vorren, T. O., J. S. Laberg, F. Blaume, J. A. Dowdeswell, N. H. Kenyon, J. Mienert, J. Rumohr, and F. Werner (1998), The Norwegian Greenland Sea continental margins: Morphology and late Quaternary sedimentary processes and environment, *Quat. Sci. Rev.*, *17*(1–3), 273–302, doi:10.1016/S0277-3791(97)00072-3.

Walczowski, W., and J. Piechura (2007), Pathways of the Greenland Sea warming, *Geophys. Res. Lett.*, *34*, L10608, doi:10.1029/2007GL029974.

Westbrook, G. K., et al. (2008), Estimation of gas hydrate concentration from multi-component seismic data at sites on the continental margins of NW Svalbard and the Storegga region of Norway, *Mar. Pet. Geol.*, *25*(8), 744–758, doi:10.1016/j.marpetgeo.2008.02.003.

Westbrook, G. K., et al. (2009), Escape of methane gas from the seabed along the West Spitsbergen continental margin, *Geophys. Res. Lett.*, *36*, L15608, doi:10.1029/2009GL039191.

Yamano, M., S. Uyeda, Y. Aoki, and T. H. Shipley (1982), Estimates of heat-flow derived from gas hydrates, *Geology*, *10*(7), 339–343, doi:10.1130/0091-7613(1982)10<339:EOHFDF>2.0.CO;2.